Supporting Information

Anomalous Carrier Transport Enhances Thermoelectricity in $HfSe_2/SnX_2$ (X = S, Se) based Heterostructures

Jipin Peter[1], Raju K Biswas[2*]

[1]Department of Physics, Faculty of Natural Sciences,

M S Ramaiah University of Applied Sciences, Bengaluru 560058, India,

[2]Department of Physics, North Eastern Regional Institute of Science and Technology, Nirjuli, Arunachal Pradesh 791109, India

****E-mail: rajukumar1718@gmail.com***

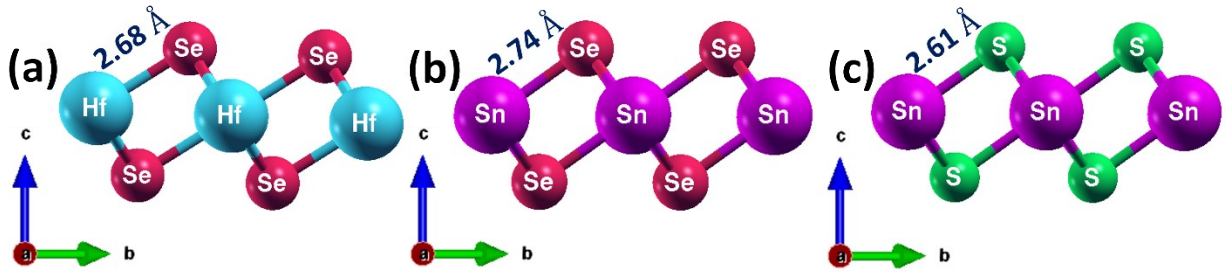

Fig. S1 Side view of the optimised crystal structure of (a) $HfSe_2$, (b) $SnSe_2$, and (c) SnS_2 monolayers.

Table S1. Lattice parameters ($a = b$), and bond length (d) of $HfSe_2$, $SnSe_2$, and SnS_2 monolayers and their corresponding homo-bilayer (HBL) and bilayer heterostructure (BLH) combinations. Also, the bandgap (eV) computed via HSE functional for all three monolayers and bilayer structures.

System	Lattice parameter, $a = b$ (Å)	Bond length, d (Å)	HSE bandgap (eV)
$HfSe_2$	3.76	2.68 (Hf – Se)	1.50 [67]
$SnSe_2$	3.84	2.74 (Sn – Se)	1.39 [11]
SnS_2	3.69	2.61 (Sn – S)	2.38 [11]
$HfSe_2$ HBL	3.74	2.65 (Hf – Se)	2.20
$HfSe_2/SnSe_2$ BLH	3.79	2.69 (Hf – Se) 2.72 (Sn – Se)	2.00

$HfSe_2/SnS_2$ BLH	3.72	2.67 (Hf – Se) 2.60 (Sn – S)	1.75

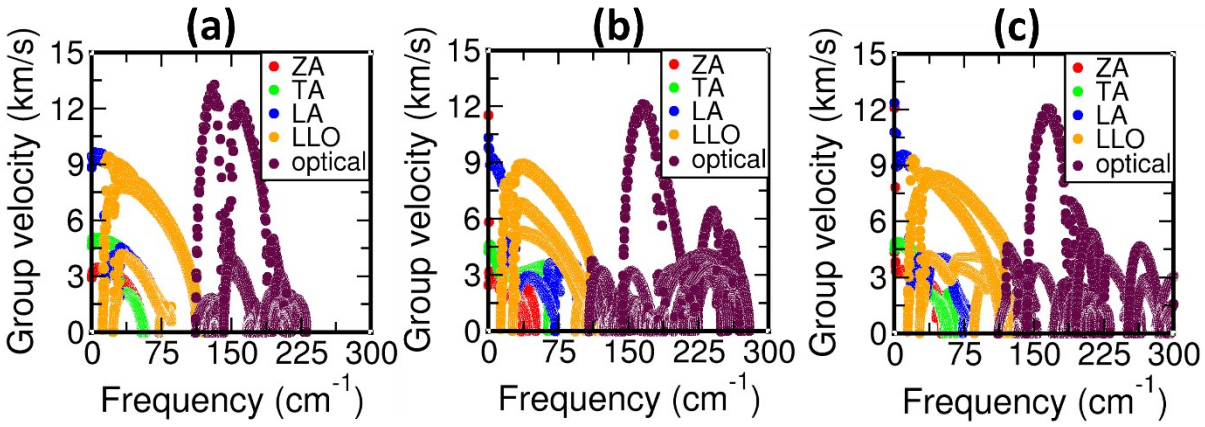

Fig. S2 Phonon group velocity for (a) $HfSe_2$ HBL, (b) $HfSe_2/SnSe_2$, and (c) $HfSe_2/SnS_2$ BLH, respectively at 300 K.

DPT formalism (Note 1)

DPT provides a formula that incorporates the effective mass of carriers to accurately estimate the longitudinal acoustic (LA) phonon-limited mobility in 2D semiconductors given as[11,57],

$$\mu_{LA} = \frac{C_{2D}\hbar^3 e}{E_1^2 (m^*)^2 k_B T} \qquad (1)$$

Where, C_{2D} is the elastic constant, $\hbar$ is the reduced Planck constant, e is the electronic charge, E_1 is the deformation potential constant, m^* is the carrier effective mass, k_B is the Boltzmann constant and T is the temperature.

Effective mass (m^*) of charge carrier is related to the curvature of the energy band in $E-K$ diagram in the reciprocal space, determined using the equation given as[11], $m^* = \hbar^2[\frac{d^2E_k}{dk^2}]^{-1}$. The deformation potential constant or carrier-phonon scattering strength (E_1) represents the energy shift observed in the band edge position due to the application of uniaxial strain. It is determined by performing a linear fitting analysis of band edge positions of the conduction band minima (CBM) and valence band maxima (VBM) as a function of lattice deformation induced by uniaxial strain. The uniaxial strain is calculated using the equation derived as[11], $\epsilon = \frac{a - a_o}{a_o}$, where ϵ is the applied uniaxial strain, a_o is the actual lattice parameter and a denotes

the lattice parameter after the application of uniaxial strain. On the other hand, elastic constant C_{2D} is derived as[11], $2(E - E_o) = C_{2D}S_o(\Delta a/a_o)^2$, where E_o and S_o represents the total energy and lattice cross sectional area of the unit cell in the absence of strain, respectively. Additionally, E denotes the total energy of the system under the influence of applied uniaxial strain.

Table S2. Calculated values of elastic constant (C_{2D}), deformation potential constant (E_1), carrier effective mass (m*), acoustic phonon limited carrier mobility (μ_{LA}) and relaxation time (τ_{LA}) at 300 K. [Here, m_o = 9.1×10^{-31} kg].

System	e/h	C_{2D} (J/m^2)	E_1 (eV)	m^* (m_o)	μ_{LA} (cm^2 V^{-1} s^{-1})	τ_{LA} (ps)
$HfSe_2$ HBL	**CB**	287.74	8.42	0.34	731	0.14
	VB		6.99	0.16	4813	0.43
$HfSe_2$/$SnSe_2$ BLH	**CB**	55.54	1.84	0.39	2229	0.49
	VB		3.24	0.19	3025	0.32
$HfSe_2$/SnS_2 BLH	**CB**	62.54	6.30	0.25	519	0.07
	VB		7.67	0.19	607	0.06

The calculated C_{2D}, E_1 and m^* values for electrons and holes for all three studied bilayer structures are presented in Table S2. In all three bilayer structures, the CBM exhibits a relatively flatter curvature than the VBM (as evident in Fig. 5), resulting in a lower effective mass for holes and consequently higher hole mobility. Interestingly, the $HfSe_2$ HBL exhibits the lowest hole effective mass ($0.16m_o$) compared to $HfSe_2$/$SnSe_2$ ($0.19m_o$) and $HfSe_2$/SnS_2 BLH ($0.19m_o$), suggesting superior hole mobility in $HfSe_2$ HBL. In contrast, for electrons, $HfSe_2$/SnS_2 BLH shows the smallest effective mass ($0.25m_o$) relative to $HfSe_2$/$SnSe_2$ BLH ($0.39m_o$) and $HfSe_2$ HBL ($0.34m_o$), implying enhanced electron transport within the system. Additionally, the calculated elastic constant reveals higher values for $HfSe_2$ HBL (287.74 J/m^2) compared to the other two BLH (as shown in Table S2), and is close to previously reported bilayer heterostructures[18]. Such high elastic constant is crucial for achieving superior carrier transport in the system. Furthermore, the deformation potential constants summarized in Table S2 is calculated by considering both tensile and compressive strain conditions. It is noteworthy that for $HfSe_2$/$SnSe_2$ BLH, the computed E_1 values are drastically lower for both electrons (1.84 eV) and holes (3.24 eV) compared to the $HfSe_2$ HBL and $HfSe_2$/SnS_2 BLH. This implies that the magnitude of carrier-phonon coupling strength is comparatively lower in $HfSe_2$/$SnSe_2$ BLH, indicating inherently higher mobility in this system compared to the other two structures. Moreover, the higher E_1 values in $HfSe_2$ HBL and $HfSe_2$/SnS_2 BLH, suggests a greater likelihood of carrier scattering events, which could ultimately lead to reduced carrier

mobility in these structures. Furthermore, we have also computed the C_{2D}, E_1 and m^* values for electrons and holes for $HfSe_2$ monolayer using the DPT formalism as shown in Table S4, which are in close agreement with the previously reported data.

Table S3. Area (A), thickness (t), dielectric constant (ε), Bose Einstein distribution (n) and Born-effective charge (Z_{MB}) are tabulated.

System	A $\times 10^{-20}$ (m²)	t $\times 10^{-10}$ m	ε	n	Z_{MB}
$HfSe_2$	36.85	3.14	13.5	1.03	6.39
$SnSe_2$	38.34	3.14	13	1.32	4.94
SnS_2	35.96	2.59	8.80	0.74	4.85

Table S4. Calculated values of elastic constant (C_{2D}), deformation potential constant (E_1), carrier effective mass (m*), longitudinal acoustic phonon limited carrier mobility (μ_{LA}), longitudinal optical phonon limited mobility (μ_{LO}) and their corresponding relaxation time τ_{LA} and τ_{LO}, respectively for $HfSe_2$ monolayer at 300 K. [Here, m_o = 9.1×10^{-31} kg].

System	e/h	C_{2D} (J/m²)	E_1 (eV)	m^* (m_o)	μ_{LA} (cm² V^{-1} s^{-1})	$\tau_{LA} \times 10^{-14}$ (s)	μ_{LO} (cm² V^{-1} s^{-1})	$\tau_{LO} \times 10^{-15}$ (s)
$HfSe_2$	**CB**	96.17	6.59	0.33	395	7.42	3.38	0.63
	VB		5.92	0.21	1252	14.95	5.31	0.63

Table S5. $p-$ type and $n-$ type Seebeck coefficient values as a function of temperatures for $HfSe_2$ HBL, $HfSe_2/SnSe_2$, and $HfSe_2/SnS_2$ bilayer heterostructures.

System	Temperature (K)	Seebeck coefficient ($\mu V/K$)	
		$p-$ type	$n-$ type
$HfSe_2$ HBL	300	1035.71	-981.09
	400	800	-711.90
	500	650.84	-559.94
	600	550.70	-462.25

	700	481.72	-388.02
	800	428.15	-337.60
$HfSe_2/SnSe_2$ BLH	300	835.71	-753.57
	400	646.28	-569.04
	500	516.03	-450.70
	600	443.90	-381.72
	700	392.15	-336.13
	800	355.74	-302.52
$HfSe_2/SnS_2$ BLH	300	434.45	-325
	400	331.86	-239.21
	500	272.33	-188.09
	600	233.82	-165.33
	700	205.81	-158.33
	800	183.47	-156.26

Table S6. $p-$ type and $n-$ type longitudinal optical phonon limited mobility (μ_{LO}) and its corresponding relaxation time values (τ_{LO}) as a function of temperatures for $HfSe_2$ monolayer, $HfSe_2$ HBL, $HfSe_2/SnSe_2$, and $HfSe_2/SnS_2$ bilayer heterostructures.

System	Temperature (K)	μ_{LO} (cm² V⁻¹ s⁻¹)		$\tau_{LO} \times 10^{-15}$ (s)	
		$p-$ type	$n-$ type	$p-$ type	$n-$ type
$HfSe_2$	300	5.31	3.38	0.63	0.63
	400	3.78	2.41	0.45	0.45
	500	2.86	1.82	0.34	0.34
	600	2.29	1.46	0.27	0.27
	700	1.92	1.22	0.22	0.22
	800	1.79	1.14	0.21	0.21
$HfSe_2$ HBL	300	10.62	6.76	0.96	1.30
	400	7.56	4.82	0.68	0.93
	500	5.72	3.64	0.52	0.70
	600	4.58	2.92	0.41	0.56
	700	3.84	2.44	0.34	0.47
	800	3.58	2.28	0.32	0.44
$HfSe_2/SnSe_2$ BLH	300	7.40	5.86	0.79	1.29
	400	5.24	4.15	0.56	0.92
	500	3.98	3.14	0.43	0.69
	600	3.19	2.53	0.34	0.56
	700	2.67	2.12	0.28	0.47
	800	2.44	1.91	0.26	0.42
$HfSe_2/SnS_2$ BLH	300	10.66	10.17	1.15	1.44
	400	7.46	7.08	0.80	1.00
	500	5.61	5.31	0.60	0.75
	600	4.46	4.22	0.48	0.60
	700	3.73	3.53	0.40	0.50
	800	3.33	3.10	0.35	0.44

Table S7. $p-$ **type and** $n-$ **type values of optimised carrier concentration and Lorenz number as a function of temperatures for $HfSe_2$ monolayer, $HfSe_2$ HBL, $HfSe_2/SnSe_2$, and $HfSe_2/SnS_2$ bilayer heterostructures.**

System	Temperature (K)	Carrier concentration (n) (10^{20} cm^{-3})		Lorenz number (WS/K^2) (10^{-8})	
		$p-$ type	$n-$ type	$p-$ type	$n-$ type
$HfSe_2$ monolayer	300	4.5	5.10	75.7	58.5
	400	11.1	12.50	42.6	32.8
	500	22.9	26.80	26.9	20.4
	600	42.0	49.00	18.0	13.8
	700	68.0	81.00	13.0	9.79
	800	96.0	111.90	9.67	7.17
$HfSe_2$ HBL	300	5	6.5	65.9	53.8
	400	11.5	16.5	39.6	29.1
	500	22.5	34.5	26.3	18.0
	600	38.5	62.0	18.7	12.2
	700	59.0	103.0	14.3	8.6
	800	78.0	144.0	11.2	6.4
$HfSe_2/SnSe_2$ BLH	300	11	11	30.6	21.0
	400	26	26	18.1	12.2
	500	54	54	11.3	7.53
	600	93	93	8.1	5.23
	700	150	150	6.0	3.77
	800	200	200	4.9	3.05
$HfSe_2/SnS_2$ BLH	300	16	26	8.59	4.8
	400	37	62	5.26	2.8
	500	72	126	3.55	1.8
	600	120	200	2.62	1.4
	700	185	255	2.02	1.29
	800	270	295	1.54	1.23

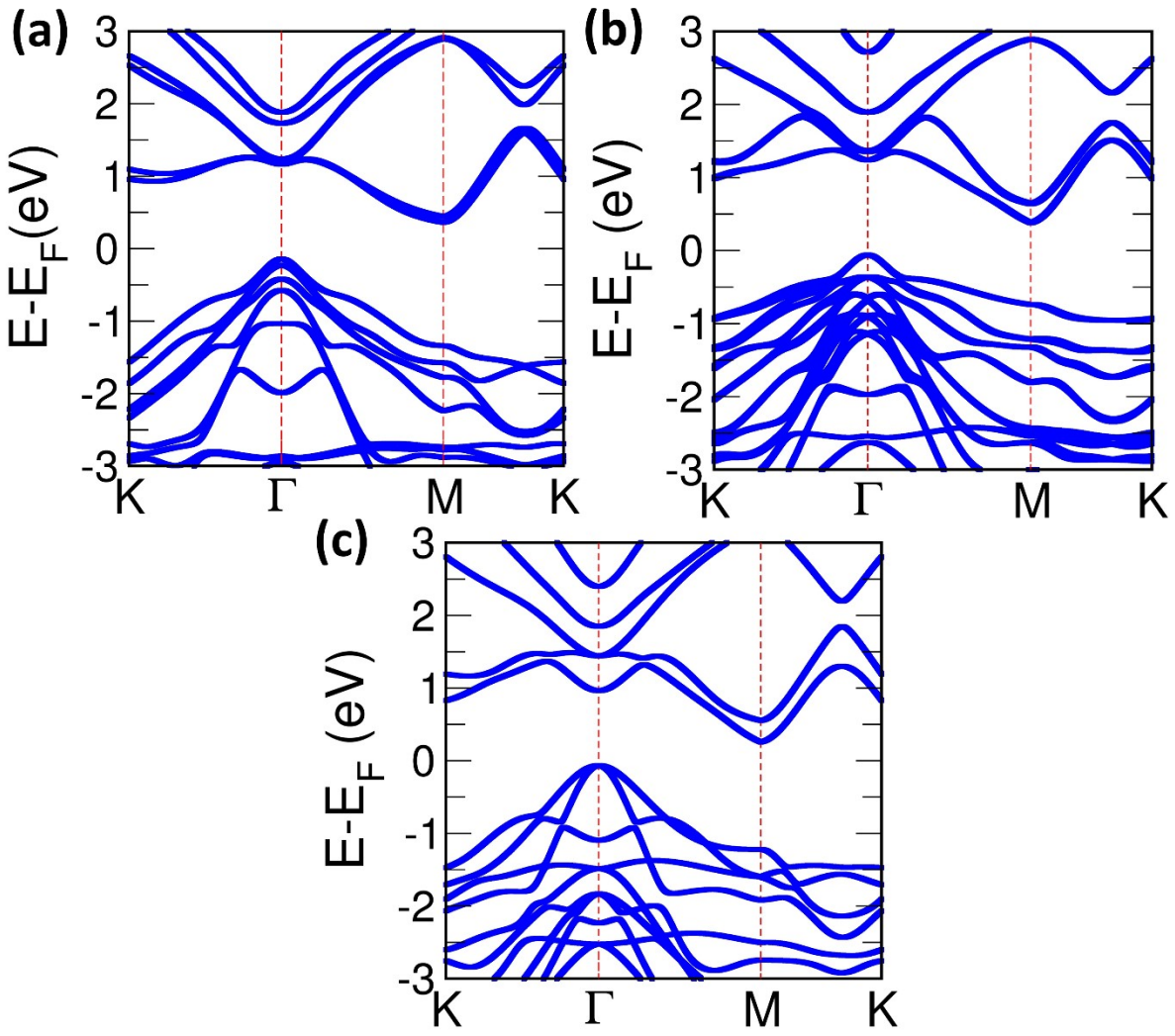

Fig S3. Electronic band structures with the inclusion of spin orbit coupling (SOC) of (a) $HfSe_2$ homo-bilayer, (b) $HfSe_2/SnSe_2$, and (c) $HfSe_2/SnS_2$ BLH, along the high symmetry points $K-\Gamma-M-K$ within the Brillouin zone (BZ).

Bader charge analysis (Note 2)

Furthermore, to give an insight into the higher binding energy of $HfSe_2/SnS_2$, we have carried out a detailed study of Bader charge analysis. The Bader charge results provide valuable insights into the degree of charge transfer and bonding nature. In an ideal ionic system, atoms often have nominal charges based on the charge transfer, with positive values for atoms that lose electrons and negative for those that gain them. However, the actual Bader charges often differ from these expected values. Furthermore, if the computed Bader charge is smaller than the nominal charge, suggest that the electron transfer is not complete, indicating the presence

of covalent character in the bonding. In our present study, we have compared the Bader charges of $HfSe_2$ homo-bilayer in conjunction with $HfSe_2/SnS_2$ BL heterostructure, to understand the underlying mechanism of the higher binding energy in the respective heterostructure.

Herein, the nominal charges of Hf and Sn are considered as +4, whereas those of Se and S are -2. In case of $HfSe_2$ homo-bilayer, the computed Bader charges for Hf and Se are +1.89 and -0.94, respectively, significantly lower than their nominal values, indicating partial charge transfer and hence a noticeable covalent character in the bonding. For the $HfSe_2/SnS_2$ bilayer (BL) heterostructure, the corresponding Bader charges for Hf and Sn are +1.86 and +1.51, while those for Se and S are -0.93 and -0.76, respectively, further confirming the presence of covalent bonding. Moreover, a closer comparison of the metal and chalcogen atoms in the $HfSe_2$ homo-bilayer and $HfSe_2/SnS_2$ BL heterostructure reveals that the deviations of the Bader charges from the nominal values are more pronounced in the heterostructure, as evident in Table S8. This suggests a stronger covalent interaction between the constituent atoms in the $HfSe_2/SnS_2$ BL heterostructure, which correlates with its higher binding energy.

Table S8. Computed Bader charge for $HfSe_2$ homo-bilayer and $HfSe_2/SnS_2$ BLH.

System	Atom	Nominal charge	Bader charge
$HfSe_2$ HBL	Hf	+4	+1.89
	Se	+2	+0.94
$HfSe_2/SnS_2$ BLH	Hf	+4	+1.86
	Sn	+4	+1.51
	Se	-2	-0.93
	S	-2	-0.76

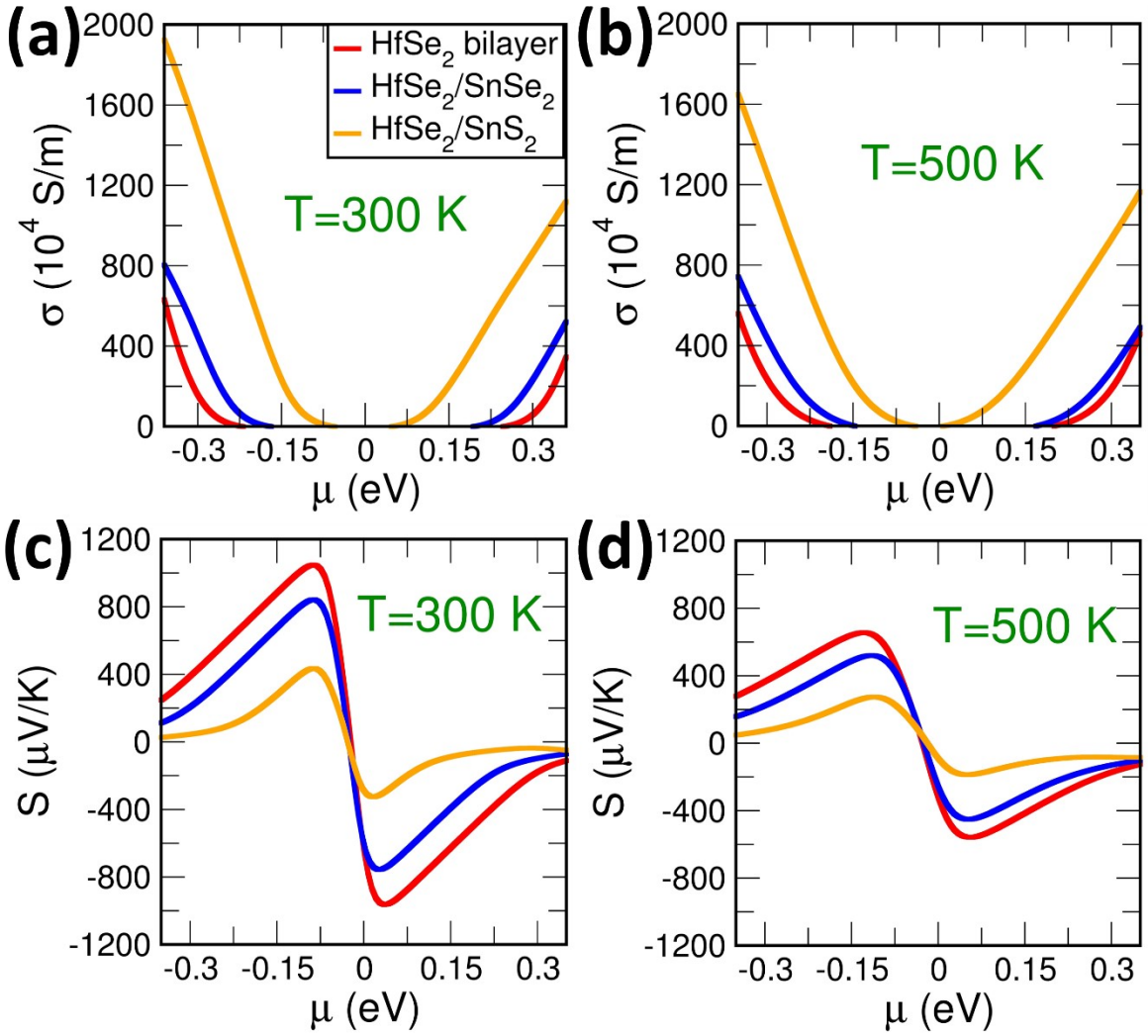

Fig. S4 (a) and (b) electrical conductivity as a function of chemical potential (μ) and (c) and (d) show computed Seebeck as a function of chemical potential (μ) at 300 K and 500 K, respectively for $HfSe_2$ monolayer and all three bilayer structures. These are the results obtained from BoltzTraP for a fixed carrier concentration of 10^{21} cm^{-3}.